Models for Extradiol Cleaving Catechol Dioxygenases: Syntheses, Structures, and Reactivities of Iron(II)−Monoanionic Catecholate Complexes

Du-Hwan Jo, Yu-Min Chiou, and Lawrence Que, Jr.*

Department of Chemistry and Center for Metals in Biocatalysis, University of Minnesota, Minneapolis, Minnesota 55455

Received October 27, 2000

Crystallographic and spectroscopic studies of extradiol cleaving catechol dioxygenases indicate that the enzyme−substrate complexes have both an iron(II) center and a monoanionic catecholate. Herein we report a series of iron(II)−monoanionic catecholate complexes, $[(L)Fe^{II}(catH)](X)$ (**1a**, L = 6-Me_3-TPA (tris(6-methyl-2-pyridylmethyl)amine), catH = CatH (1,2-catecholate monoanion); **1b**, L = 6-Me_3-TPA, catH = DBCH (3,5-di-*tert*-butyl-1,2-catecholate monoanion); **1c**, L = 6-Me_2-bpmcn (*N*,*N*′-dimethyl-*N*,*N*′-bis(6-methyl-2-pyridylmethyl)-*trans*-1,2-diaminocyclohexane), catH = CatH; **1d**, L = 6-Me_2-bpmcn, catH = DBCH), that model such enzyme complexes. The crystal structure of $[(6\text{-}Me_2\text{-bpmcn})Fe^{II}(DBCH)]^+$ (**1d**) shows that the DBCH ligand binds to the iron asymmetrically as previously reported for **1b**, with two distinct Fe−O bonds of 1.943(1) and 2.344(1) Å. Complexes **1** react with O_2 or NO to afford blue-purple iron(III)−catecholate dianion complexes, $[(L)Fe^{III}(cat)]^+$ (**2**). Interestingly, crystallographically characterized **2d**, isolated from either reaction, has the *N*-methyl groups in a *syn* configuration, in contrast to the *anti* configuration of the precursor complex, so epimerization of the bound ligand must occur in the course of isolating **2d**. This notion is supported by the fact that the UV−vis and EPR properties of in situ generated **2d**(*anti*) differ from those of isolated **2d**(*syn*). While the conversion of **1** to **2** in the presence of O_2 occurs without an obvious intermediate, that in the presence of NO proceeds via a metastable $S = {}^3/_2$ $[(L)Fe(catH)(NO)]^+$ adduct **3**, which can only be observed spectroscopically but not isolated. Intermediates **3a** and **3b** subsequently disproportionate to afford two distinct complexes, $[(6\text{-}Me_3\text{-TPA})Fe^{III}(cat)]^+$ (**2a** and **2b**) and $[(6\text{-}Me_3\text{-TPA})Fe(NO)_2]^+$ (**4**) in comparable yield, while **3d** converts to **2d** in 90% yield. Complexes **2b** and *anti*-**2d** react further with O_2 over a 24 h period and afford a high yield of cleavage products. Product analysis shows that the products mainly derive from intradiol cleavage but with a small extent of extradiol cleavage (89:3% for **2b** and 78:12% for *anti*-**2d**). The small amounts of the extradiol cleavage products observed may be due to the dissociation of an α-methyl substituted pyridyl arm, generating a complex with a tridentate ligand. Surprisingly, *syn*-**2d** does not react with O_2 over the course of 4 days. These results suggest that there are a number of factors that influence the mode and rate of cleavage of catechols coordinated to iron centers.

Introduction

The catechol dioxygenases are non-heme enzymes that catalyze the oxidative cleavage of catechols in the final step for the degradation of natural aromatic molecules into aliphatic products.[1] Cleavage of the C−C bond adjacent to the enediol unit (extradiol) represents the more common oxidative cleavage pathway in nature, utilizing enzymes that have Fe(II) or Mn(II) in the active site. The crystal structures of these enzymes reveal a square pyramidal geometry at the iron center that consists of three endogenous ligands (two histidines and one glutamate) in a facial array and two solvent molecules.[2] In addition, the structures of the enzyme−substrate (E·S) complexes of 2,3-dihydroxybiphenyl 1,2-dioxygenase (1,2-BphC) and protocatechuate 4,5-dioxygenase (4,5-PCD) reveal that the iron active site adopts a 5-coordinate structure with the three endogenous ligands and a chelated catecholate.[3] While the catecholate coordinates in a bidentate fashion, it does so asymmetrically with one $Fe-O_{cat}$ bond 0.2 Å shorter than the other. A similar bond asymmetry has also been observed in EXAFS studies of the catechol 2,3-dioxygenase (2,3-CTD)-catechol complex[4] and ascribed to a monoanionic substrate. The remaining coordination site is presumably reserved for O_2, as suggested by the binding of nitric oxide (NO) as a dioxygen surrogate,[1a,5] which converts the normally EPR-silent mononuclear high-spin Fe(II) center ($S = 2$) into an EPR active $S = {}^3/_2$ species. This ternary

* To whom correspondence should be sent. Fax: (+1) 612-624-7029. E-mail: que@chem.umn.edu.

(1) (a) Lipscomb, J. D.; Orville, A. M. *Metal Ions Biol. Syst.* **1992**, *28*, 243−298. (b) Que, L., Jr. In *Bioinorganic Catalysis*, 2nd ed.; Reedijk, J., Bouwman, E., Eds.; Marcel Dekker: New York, 1999; pp 269−321. (c) Solomon, E. I.; Brunold, T. C.; Davis, M. I.; Kemsley, J. N.; Lee, S.-K.; Lehnert, N.; Neese, F.; Skulan, A. J.; Yang, Y.-S.; Zhou, J. *Chem. Rev.* **2000**, *100*, 235−349. (d) Krüger, H.-J. In *Biomimetic Oxidations Catalyzed by Transition Metal Complexes*; Meunier, B., Ed.; Imperial College Press: London, 2000; pp 363−413.

(2) (a) Han, S.; Eltis, L. D.; Timmis, K. N.; Muchmore, S. W.; Bolin, J. T. *Science* **1995**, *270*, 976−980. (b) Kita, A.; Kita, S.-I.; Fusisawa, I.; Inaka, K.; Ishida, T.; Horiiki, K.; Nozaki, M.; Miki, K. *Structure* **1999**, *7*, 25−34.

(3) (a) Sugiyama, K.; Senda, T.; Narita, H.; Yamamoto, T.; Kimbara, K.; Fukuda, M.; Yano, K.; Mitsui, Y. *Proc. Jpn Acad., Ser. B* **1995**, *71*, 32−35. (b) Senda, T.; Sugiyama, K.; Narita, H.; Yamamoto, T.; Kimbara, K.; Fukuda, M.; Sato, M.; Yano, K.; Mitsui, Y. *J. Mol. Biol.* **1996**, *255*, 735−752. (c) Sugimoto, K.; Senda, T.; Aoshima, H.; Masai, E.; Fukuda, M.; Mitsui, Y. *Structure* **1999**, *7*, 953−965.

(4) Shu, L.; Chiou, Y.-M.; Orville, A. M.; Miller, M. A.; Lipscomb, J. D.; Que, L., Jr. *Biochemistry* **1995**, *34*, 6649−6659.

(5) (a) Arciero, D. M.; Lipscomb, J. D.; Huynh, B. H.; Kent, T. A.; Münck, E. *J. Biol. Chem.* **1983**, *258*, 14981−14991. (b) Arciero, D. M.; Orville, A. M.; Lipscomb, J. D. *J. Biol. Chem.* **1985**, *260*, 14035−14044. (c) Arciero, D. M.; Lipscomb, J. D. *J. Biol. Chem.* **1986**, *261*, 2170−2178.

10.1021/ic001185d CCC: $20.00
Published on Web 05/17/2001

enzyme−substrate−NO complex has been proposed to be a model for the iron−dioxygen intermediate in the enzymatic reaction mechanism.[5b−c]

To date, several synthetic Fe(III)−catecholate complexes serve as functional models for extradiol cleaving dioxygenases,[6] but there is only one mononuclear Fe(II)−catecholate complex that is structurally characterized, [(6-Me_3-TPA)Fe^{II}(DBCH)]-(ClO_4), a result reported in an earlier communication.[7] In this paper, we report the synthesis and characterization of a series of mononuclear Fe(II)−catecholate complexes, [(L)Fe^{II}(catH)](X) (L = 6-Me_3-TPA, 6-Me_2-bpmcn; catH = CatH, DBCH; X = counterions)[8] and their reactivities toward O_2 and NO in order to evaluate the plausibility of structural and reactivity features postulated for the extradiol cleaving dioxygenases.

Experimental Section

Materials and Procedures. Reagents were purchased from commercial sources and used as received unless otherwise noted. The catechols ($CatH_2$ and $DBCH_2$) were purified by sublimation or recrystallization from hexane. Preparation and handling of air-sensitive materials were carried out under an argon atmosphere using standard Schlenk techniques or in an anaerobic glovebox. All solvents were distilled using standard methods under argon. Nitric oxide (99+%, Matheson Gas Products, Inc.) was passed through a column of NaOH pellets to prevent nitric acid contamination and the line purged with argon gas for 30 min before using to ensure removal of any adventitious O_2.

6-Me_3-TPA and 6-Me_2-bpmcn. 6-Me_3-TPA was synthesized according to published procedures,[9] while 6-Me_2-bpmcn was prepared by the following method. To an ethanolic solution (100 mL) of 6-methyl-pyridine 2-carboxaldehyde (4.8 g, 20 mmol) was added racemic *trans*-1,2-diaminocyclohexane (2.28 g, 40 mmol), and the mixture was stirred for 2 h at room temperature. The solution was concentrated to give crystals of *N*,*N*′-bis(6-methyl-2-pyridylmethyl)-1,2-cyclohexadiimine, which was filtered and washed with cold ethanol. Yield: 6.08 g (90%). ^{1}H NMR ($CDCl_3$, ppm): 8.30(s, 2H, N=C*H*), 7.70(d, 2H, 3*H*-py), 7.52(t, 2H, 4*H*-py), 7.07(d, 2H, 5*H*-py), 3.51(t, 2H, NC*H*), 2.52(s, 6H, py-CH_3), 1.81(m, 6H), 1.50(s, 2H). ^{13}C NMR ($CDCl_3$, ppm): 161.6(N=*C*H), 157.6, 154.14, 136.5, 124, 118, 73.5-(N*C*H), 32.6(py-*C*H_3), 24.3, 24.2. The reduction of the di-imine was then carried out using KBH_4 in dry methanol. To the methanolic solution (50 mL) of di-imine (3.2 g, 10 mmol) was slowly added excess KBH_4 and the mixture was refluxed for 1 h. The solution was cooled and then quenched with cold water (20 mL). Following chloroform extraction (3 × 50 mL), the organic layer was dried with Na_2SO_4. Removal of chloroform yielded the oily *N*,*N*′-bis(6-methyl-2-pyridylmethyl)-1,2-cyclohexadiamine. Yield: 3.07 g (95%). ^{1}H NMR ($CDCl_3$, ppm): 7.50(t, 2H, 4*H*-py), 7.21(d, 2H, 3*H*-py), 6.97(d, 2H, 5*H*-py), 4.01(d, 2H, AB, J = 14 Hz; NCH_2), 3.97(d, 2H, AB, J = 14 Hz; NCH_2), 2.51(s, 6H, py-CH_3), 2.31(2H, NC*H*), 2.13(2H), 1.70(2H), 1.04−1.26-(m, 4H). ^{13}C NMR ($CDCl_3$, ppm): 159.9, 157.5, 121.1, 119.0, 61.3-(N*C*H$_2$), 52.4(N*C*H), 31.6(py-*C*H_3), 24.9, 24.4. 6-Me_2-bpmcn ligand was then obtained by methylation of the secondary di-amine using formic acid−formaldehyde. A mixture of the secondary amine (1.61 g, 5 mmol), formic acid (15 mL, 88%), and formaldehyde (15 mL, 37%) was refluxed at 90 °C with stirring for 3 days. The solution was cooled in an ice bath and then brought to pH 12 with a saturated solution of NaOH. The resulting solution was extracted with chloroform, dried over Na_2SO_4, and evaporated to give a light yellow oil, *trans*-*N*,*N*′-dimethyl-*N*,*N*′-bis(6-methyl-2-pyridylmethyl)-1,2-cyclohexadiamine. Yield: 1.41 g (80%). ^{1}H NMR ($CDCl_3$, ppm): 7.49(t, 2H, 4*H*-py), 7.41(d, 2H, 3*H*-py), 6.95(d, 2H, 5*H*-py), 3.90(d, 2H, AB, J = 9.6 Hz; NCH_2), 3.75(d, 2H, AB, J = 9.6 Hz; NCH_2), 2.66(t, 2H, NC*H*), 2.53-(s, 6H; py-CH_3), 2.30(s, 6H; NCH_3), 1.97(d, 2H), 1.76(d, 2H), 1.1∼1.4-(m, 4H). ^{13}C NMR ($CDCl_3$, ppm): 160, 157, 136.5, 121, 119.7, 64.6(N*C*H), 60.3(N*C*H$_2$), 36.6(py*C*H$_3$), 25.8, 25.6, 24.4(N*C*H$_3$).

Metal Complexes. Caution. Perchlorate salts of metal complexes with organic ligands are potentially explosive and should be handled with great caution. NO is a poisonous gas and should only be used with proper ventilation.

[(6-Me_3-TPA)Fe^{II}(CatH)](ClO_4) (1a). A methanolic solution of 6-Me_3-TPA (0.36 g, 1.0 mmol) was added to a methanol solution (30 mL) of $Fe(ClO_4)_2$·$6H_2O$ (0.36 g, 1.0 mmol) and stirred for 10 min. To this solution was slowly added a methanolic solution of $CatH_2$ (0.11 g, 1.0 mmol) and triethylamine (0.10 g, 1.0 mmol). The resulting yellow solution was stirred for 30 min under argon and the yellow microcrystalline product was filtered and dried under vacuum. Yield: 0.56 g (90%). Anal. Calcd. for **1a**, $C_{27}H_{29}ClFeN_4O_6$: C, 54.33; H, 4.90; N, 9.39, Cl, 5.94. Found: C, 54.16; H, 4.70; N, 9.30; Cl, 6.16. UV−vis [λ_{max}, nm (ϵ, $M^{-1}cm^{-1}$) in CH_3CN]: 386 (2000).

[(6-Me_3-TPA)Fe^{II}(DBCH)](ClO_4) (1b). This compound was prepared in a manner analogous to that described for **1a** except that $DBCH_2$ (0.22 g, 1.0 mmol) was used in place of $CatH_2$.[7] Yield: 0.62 g (82%). Crystallographic quality crystals were obtained by vapor diffusion of Et_2O into an ethanol solution of **1b**. Anal. Calcd. for **1b**·EtOH, $C_{37}H_{51}ClFeN_4O_7$: C, 58.85; H, 6.81; N, 7.42, Cl, 4.69. Found: C, 58.58; H, 6.81; N, 7.37; Cl, 4.93. UV−vis [λ_{max}, nm (ϵ, $M^{-1}cm^{-1}$) in CH_3CN]: 395 (2200).

[(6-Me_2-bpmcn)Fe^{II}(CatH)](CF_3SO_3) (1c). A CH_2Cl_2 solution of 6-Me_2-bpmen (0.353 g, 1.0 mmol) was added to a CH_2Cl_2 solution (30 mL) of $Fe(CF_3SO_3)_2$ (0.354 g, 1.0 mmol) and stirred for 10 min. To this solution was slowly added a CH_2Cl_2 solution of $CatH_2$ (0.11 g, 1.0 mmol) and triethylamine (0.10 g, 1.0 mmol). The mixture was stirred for 30 min and layered with diethyl ether to give greenish-yellow crystals. Yield: 0.43 g (65%). Anal. Calcd. for **1c**·Et_2O, $C_{33}H_{47}F_3FeN_4O_6S$: C, 53.51; H, 6.40; N, 7.57, S, 4.33. Found: C, 53.35; H, 5.50; N, 7.73; S, 4.40. UV−vis [λ_{max}, nm (ϵ, $M^{-1}cm^{-1}$) in CH_3CN]: 380 (900).

[(6-Me_2-bpmcn)Fe^{II}(DBCH)](CF_3SO_3) (1d). This compound was prepared in a manner analogous to that described for **1c** except that $DBCH_2$ (0.22 g, 1.0 mmol) was used in place of $CatH_2$. Crystallographic quality crystals were obtained by vapor diffusion of diethyl ether into a CH_2Cl_2 solution. Yield: 0.55 g (70%). Anal. Calcd. for **1d**·$0.5CH_2Cl_2$, $C_{37.5}H_{54}ClF_3FeN_4O_5S$: C, 54.85; H, 6.63; N, 6.82, S, 3.90. Found: C, 55.14; H, 6.62; N, 6.62; S, 3.90. UV−vis [λ_{max}, nm (ϵ, $M^{-1}cm^{-1}$) in CH_3CN]: 384 (1100).

[(6-Me_3-TPA)Fe^{III}(Cat)](BPh_4) (2a). Complex **1a** (60 mg, 0.1 mmol) in 20 mL methanol was reacted with NO, turning the yellow solution brown in less than 1 min. Addition of $NaBPh_4$ to the methanol solution, followed by vapor diffusion of diethyl ether at room temperature for 2∼3 days, resulted in the formation of two distinct crystal forms in comparable yields, purple-blue needle crystals of **2a**, and brown prismatic crystals of **4** (see below). The crystals of **2a** were manually separated from the brown crystals of **4**. Anal. Calcd. for **2a**, $C_{51}H_{48}BFeN_4O_2$: C, 75.10; H, 5.93; N, 6.87. Found: C, 74.85; H, 5.89; N, 7.01. UV−vis [λ_{max}, nm (ϵ, $M^{-1}cm^{-1}$) in CH_3CN]: 540 (2100), 940 (3200).

[(6-Me_3-TPA)Fe^{III}(DBC)](ClO_4) (2b). Complex **1b** (71 mg, 0.1 mmol) in 20 mL CH_2Cl_2 was reacted with NO to form a brown solution. Diffusion of hexane into this solution at room temperature for 3−4 days resulted in the formation of two distinct crystal forms, blue crystals of **2b** and brown crystals of **4** (see below). The crystals of **2b** were manually separated from the brown crystals of **4**. Anal. Calcd. for **2b,**

(6) (a) Dei, A.; Gatteschi, D.; Pardi, L. *Inorg. Chem.* **1993**, *32*, 1389−1395. (b) Ito, M.; Que, L., Jr. *Angew. Chem., Int. Ed. Engl.* **1997**, *36*, 1342−1344. (c) Ogihara, T.; Hikichi, S.; Akika, M.; Moro-oka, Y. *Inorg. Chem.* **1998**, *37*, 2614−2615.

(7) Chiou, Y.-M.; Que, L., Jr. *Inorg. Chem.* **1995**, *34*, 3577−3578.

(8) Abbreviations: BF, benzoylformate; bpeen, *trans*-*N*,*N*′-diethyl-*N*,*N*′-bis(2-pyridylmethyl)-1,2-ethylenediamine; BPG, *N*,*N*-bis(2-pyridylmethyl)glycine; bpmcn, *trans*-*N*,*N*′-dimethyl-*N*,*N*′-bis(2-pyridylmethyl)-1,2-cyclohexadiamine; bpmen, *trans*-*N*,*N*′-dimethyl-*N*,*N*′-bis(2-pyridylmethyl)-1,2-ethylenediamine; cat, catecholate dianion (Cat or DBC); catH, catecholate monoanion (DBCH or CatH); CatH, 1,2-catecholate monoanion; DBCH, 3,5-di-*tert*-butyl-1,2-catecholate monoanion; 6-Me_2-bpmcn, *trans*-*N*,*N*′-dimethyl-*N*,*N*′-bis(6-methyl-2-pyridylmethyl)-1,2-cyclohexadiamine; 6-Me_3-TPA, tris(6-methyl-2-pyridylmethyl)amine; NTA, *N*,*N*-bis(carboxymethyl)glycine; TPA, tris(2-pyridylmethyl)-amine; Tp^{i-Pr2}, hydrotris(3,5-di-*iso*-propyl-1-pyrazolyl)borate.

(9) Da Mota, M. M.; Rodgers, J.; Nelson, S. M. *J. Chem. Soc. A* **1969**, 2036−2044.

$C_{35}H_{44}ClFeN_4O_6$: C, 59.37; H, 6.26; N, 7.91, Cl, 5.01. Found: C, 59.54; H, 6.08; N, 7.76; Cl, 5.23. UV−vis [λ_{max}, nm (ϵ, $M^{-1}cm^{-1}$) in CH_3CN]: 600 (2200), 1020 (3400).

[(6-Me$_2$-bpmcn)Fe^{III}(Cat)](CF$_3$SO$_3$) (2c). Complex **1c** (78 mg, 0.1 mmol) was exposed to O_2 in CH_2Cl_2 to form **2c**. Diffusion of diethyl ether into this solution at 4 °C for several months afforded microcrystals of **2c**. UV−vis [λ_{max}, nm (ϵ, $M^{-1}cm^{-1}$) in CH_3CN]: 535 (2300), 874 (3000).

[(6-Me$_2$-bpmcn)Fe^{III}(DBC)](CF$_3$SO$_3$) (2d). Complex **1d** (78 mg, 0.1 mmol) was reacted with NO in 20 mL CH_2Cl_2. Diffusion of hexane into this solution at room temperature for 3−4 days resulted in the formation of purple-blue crystals of **2d** in excellent yield (70 mg, 90%). Anal. Calcd. for **2d**, $C_{37}H_{52}F_3FeN_4O_5S$: C, 57.14; H, 6.74, N; 7.20, S; 4.12. Found: C, 56.68; H, 6.77; N, 6.81; S, 3.88. UV−vis [λ_{max}, nm (ϵ, $M^{-1}cm^{-1}$) in CH_3CN]: 598 (2200), 950 (3100). Complex **2d** was also obtained by brief exposure of a solution of **1d** (0.39 g, 0.5 mmol) in 20 mL CH_2Cl_2 to O_2, turning the solution blue in color. Addition of diethyl ether to this solution and storage at 4 °C for 2 months afforded blue crystals that had the same spectroscopic properties as isolated **2d** from the reaction of **1d** with NO. Complex **2d** was also obtained by direct synthesis. To a CH_3CN (20 mL) solution of $Fe(ClO_4)_3 \cdot 10H_2O$ (0.267 g, 0.5 mmol) was added a CH_3CN solution of 6-Me$_2$-bpmcn (0.177 g, 0.5 mmol). This solution was stirred for 30 min, then $DBCH_2$ (0.11 g, 0.5 mmol) and triethylamine (0.20 g, 1 mmol) were added. After stirring for 2 h, the reaction solution was evaporated to dryness. The solid residue was dissolved in CH_2Cl_2, and this solution was layered with diethyl ether; upon standing at 4 °C, diffraction quality crystals of the perchlorate salt of **2d** were obtained. The structure of the perchlorate salt (unpublished data) matched that of the triflate salt reported in this paper.

[(6-Me$_3$-TPA)Fe(NO)$_2$](X) (4). Complex **4** was obtained from the reaction of **1a** or **1b** with NO. As described earlier, these reactions gave a mixture of products, **4** and **2a** or **2b**, which could be separated manually. Anal. Calcd. for **4** (X = ClO_4), $C_{21}H_{24}ClFeN_6O_6$: C, 46.05; H, 4.42; N, 15.34, Cl, 6.47. Found: C, 45.75; H, 4.65; N, 15.54; Cl, 6.37. Anal. Calcd. for **4** (X = BPh_4) $C_{45}H_{44}BFeN_6O_2$: C, 70.40; H, 5.78; N, 10.95. Found: C, 70.50; H, 5.86; N, 11.13. UV−vis [λ_{max}, nm (ϵ, $M^{-1}cm^{-1}$) in CH_3CN]: 332 (sh, 1700), 374 (sh, 1300), 460 (sh, 360), 820 (200) nm. IR (cm^{-1}, KBr pellet): ν(NO) 1801(s), 1726(s). EPR (CH_3CN at 5 K): $g = 2.02$.

Crystallographic Studies. [(6-Me$_2$-bpmcn)Fe^{II}(DBCH)](CF$_3$SO$_3$) (1d) and [(6-Me$_2$-bpmcn)Fe^{III}(DBC)](CF$_3$SO$_3$) (2d). Yellow (**1d**) and purple-blue (**2d**) crystals suitable for X-ray diffraction studies were grown from CH_2Cl_2/diethyl ether and CH_2Cl_2/hexane solvent pairs, respectively. The crystals were attached to glass fibers with heavyweight oil and mounted on a Siemens SMART system for data collection at 173(2) K. An initial set of cell constants was calculated from reflections harvested from three sets of 20 frames. These initial sets of frames are oriented such that orthogonal wedges of reciprocal space were surveyed. This produces orientation matrixes determined from 204 reflections for **1d** and 62 reflections for **2d**. Final cell constants are calculated from a set of 8192 (for **1d**) and 3977 (for **2d**) strong reflections from actual data collection. Crystallographic data and experimental conditions are summarized in Table 1. Both structures were solved by direct methods. All non-hydrogen atoms were refined anisotropically and hydrogen atoms were placed in ideal positions and refined as riding atoms with relative isotropic displacement parameters. The final full matrix least squares refinement coverged to R1 = 0.0373, wR2 = 0.0909 for **1d** and R1 = 0.0563, wR2 = 0.1213 for **2d**.

[(6-Me$_3$-TPA)Fe^{III}(Cat)](BPh$_4$) (2a) and [(6-Me$_3$-TPA)Fe(NO)$_2$](ClO$_4$) (4). Crystal data for a purple-blue crystal of **2a** and a red-brown prismatic crystal of **4** individually mounted on glass fibers with heavyweight oil were collected at 297 (2) and 177 (2) K, respectively. Crystallographic data and experimental conditions are listed in Table 1. Measurements were carried out on an Enraf-Nonius CAD-4 diffractometer with graphite monochromated Mo Kα radiation. Cell constants were obtained from a least-squares refinements of the setting angles for 50 reflections for **2a** and for 46 reflections for **4**. Lorentz and polarization corrections were applied to the data and absorption corrections based on ψ scans were carried out a maximum 2θ value of 52.0° for **2a** and 56.0° for **4**. Both structures were solved by direct methods. All non-hydrogen atoms were refined with anisotropic thermal parameters. Hydrogen atoms were placed at calculated positions and refined as riding atoms. Final cycles of refinement converged with discrepancy indices of R1 = 0.0482, wR2 = 0.0956 for **2a** and R1 = 0.0539, wR2 = 0.1290 for **4**.

Physical Measurements. Elemental analyses (C, H, Cl, N, S) were performed at M-H-W Laboratories (Phoenix, AZ). ^{1}H- and ^{13}C NMR spectra were recorded on a Varian VXR-300 or IBM AC-300 spectrometer at room temperature. X-band EPR spectra were performed at liquid helium temperature on a Varian E-109 spectrometer or a Bruker E-500 spectrometer equipped with an Oxford ESR-10 cryostat. The magnetic field was calibrated with a gaussmeter, and the microwave frequency was measured with a counter. UV−visible spectra were recorded on a Hewlett-Packard 8452 or 8453 diode array spectrometer. Infrared spectra of KBr pellets were obtained on a Mattson Polaris FT-IR spectrometer. Standard organic product analyses were performed using a Hewlett-Packard HP-6890 Series gas chromatograph equipped with a J & W Scientific DB-5 column and a flame ionization detector or a reverse-phase isocratic HPLC (Waters 6000A isocratic system; Kratos 769Z variable wavelength detector, 240 nm; Whatman Partisil ODS-5 C18 column). Mass spectral analysis was carried out on a Hewlett-Packard Model 5989B mass spectrometer.

Oxygenation Studies. Reactivity studies were performed in CH_3CN under an O_2 atmosphere. In a typical stoichoimetric reaction, complex **1** (0.05 mmol) was reacted with O_2 in 20 mL of solvent. The pale greenish-yellow color of the complex turned intense purple-blue immediately, and the resulting solution gradually faded to yellow-brown as the reaction proceeded. The solution was concentrated and extracted with diethyl ether (3 × 5 mL). The solid residue was acidified with 3 N HCl to pH 3 to effect decomposition of the metal complexes and extracted with diethyl ether (3 × 5 mL). The combined ether extract was dried over anhydrous Na_2SO_4 and concentrated and the extract was then submitted for GC, GC-MS (EI), and reverse-phase isocratic HPLC separation (conditions are the same as previously reported[10]).

Characterization of Oxygenation Products. The intradiol cleavage products, 3,5-di-*tert*-butyl-1-oxacyclohepta-3,5-diene-2,7-dione and 3,5-di-*tert*-butyl-5-carboxymethyl-2-furanone, were identified by using GC-MS (EI) and ^{1}H- and ^{13}C NMR techniques. These data are consistent with the published data,[11] and authentic compounds were prepared by treating 3,5-di-*tert*-butyl-*o*-benzoquinone with excess *m*-chloroperoxybenzoic acid at 0 °C.[12] The two structural isomers of the extradiol cleavage products, 3,5- and 4,6-di-*tert*-butyl-2-pyrone, were also identified by using the same spectroscopic methods and compared with the authentic compounds prepared according to the published procedures.[13]

O_2 Uptake. Manometric measurements of dioxygen uptake were carried out using a similar apparatus as described previously.[14] The number of moles of O_2 taken up was calculated with the ideal gas law. The absolute accuracy of the reaction system was checked by using Vaska's complex, $[IrCl(CO)(PPh_3)_2]$ (O_2/Ir = 1:1).[15] For three replicate runs using 0.2 mmol of **1b** at 22 °C, the O_2:Fe ratio was found to be 1.3(1).

Results and Discussion

The Fe(II)−catecholate complexes containing the tetradentate ligands 6-Me$_3$-TPA and 6-Me$_2$-bpmcn (**1**) have been synthesized to serve as models for the enzyme−substrate complexes of the extradiol cleaving catechol dioxygenases. Treatment of $Fe^{II}X_2$ (X = ClO_4 or CF_3SO_3) with equimolar quantities of L, catechol

(10) Cox, D. D.; Que, L., Jr. *J. Am. Chem. Soc.* **1988**, *110*, 8085−8092.
(11) Jang, H. G.; Cox, D. D.; Que, L., Jr. *J. Am. Chem. Soc.* **1991**, *113*, 9200−9204.
(12) Demmin, T. R.; Rogić, M. M. *J. Org. Chem.* **1980**, *45*, 1153−1156.
(13) Matsumoto, M.; Kuroda, K. *J. Am. Chem. Soc.* **1982**, *104*, 1433−1434.
(14) (a) Karlin, K. D.; Cruse, R. W.; Gultneh, Y.; Farooq, A.; Hayes, J. C.; Zubieta, J. *J. Am. Chem. Soc.* **1987**, *109*, 2668−2679. (b) Tolman, W. B.; Liu, S.; Bentsen, J. G.; Lippard, S. J. *J. Am. Chem. Soc.* **1991**, *113*, 152−164.
(15) Vaska, L. *Science* **1963**, *140*, 809−810.

Table 1. Crystallographic Data of **1d**, **2a**, **2d**, and **4**

	1d·0.5CH_2Cl_2	**2a**
empirical formula	$C_{37.5}H_{54}ClF_3FeN_4O_5S$	$C_{51}H_{48}BFeN_4O_2$
formula weight (g/mol)	821.21	815.59
crystal habit, color	block, yellow	prism, purple-blue
crystal system	monoclinic	triclinic
space group	$P2_1/c$	$P\bar{1}$
a (Å)	10.3726(5)	9.696(4)
b (Å)	21.903(1)	14.704(7)
c (Å)	17.6723(8)	15.315(13)
α, deg	90	89.65(7)
β, deg	97.121(1)	85.33(7)
γ, deg	90	81.43(4)
V (Å^3)	3984.0(3)	2152(2)
Z	4	2
D_{calc} (g/cm^3)	1.369	1.259
temperature (K)	173(2)	297(2)
θ range (deg)	1.49 ∼ 27.49	1.33 ∼ 25.98
hkl ranges	−13, −28, −22 to 12, 27, 21	0, −17, −18 to 11, 18, 18
no. of reflections collected	31610	8941
no. of unique reflections	8991 (R_{int} = 0.0306)	8415 (R_{int} = 0.0359)
radiation (Å)	Mo−Kα, 0.71073	Mo−Kα, 0.71073
absorption coefficient (mm^{-1})	0.558	0.396
R1/wR2 ($I > 2\sigma(I)$)[a]	0.0373/0.0909	0.0482/0.0956
R1/wR2 (all data)	0.0529/0.0965	0.0812/0.1094

	2d	**4**
empirical formula	$C_{37}H_{52}F_3FeN_4O_5S$	$C_{21}H_{24}ClFeN_6O_6$
formula weight (g/mol)	777.74	547.76
crystal habit, color	needle, purple	prism, red-brown
crystal system	monoclinic	monoclinic
space group	$P2_1/n$	$P2_1/n$
a (Å)	8.517(1)	11.934(4)
b (Å)	50.379(6)	16.540(15)
c (Å)	9.874(1)	12.408(4)
α, deg	90	90
β, deg	105.938(3)	101.01(3)
γ, deg	90	90
V (Å^3)	4073.8(9)	2404(3)
Z	4	4
D_{calc} (g/cm^3)	1.268	1.513
temperature (K)	173(2)	177(2)
θ range (deg)	1.62 ∼ 27.51	2.08 ∼ 28.0
hkl ranges	−10, −59, −12 to 11, 65, 10	−7, −21, −16 to 15, 21, 16
no. of reflections collected	25658	5800
no. of unique reflections	9260 (R_{int} = 0.0653)	5800 (R_{int} = 0.033)
radiation (Å)	Mo−Kα, 0.71073	Mo−Kα, 0.71073
absorption coefficient (mm^{-1})	0.479	0.788
R1/wR2 ($I > 2\sigma(I)$)[a]	0.0563/0.1213	0.0539/0.1290
R1/wR2 (all data)	0.1115/0.1380	0.0976/0.1512

[a] $R1 = \sum||F_o| - |F_c||/\sum|F_o|$. $wR2 = [\sum[w(F_o^2 - F_c^2)^2]/\sum[w(F_o^2)^2]]^{1/2}$, where $w = q/\sigma^2(F_o^2) + (a*P)^2 + b*P$.

($catH_2$), and triethylamine under N_2 affords pale green solutions that yield [(L)Fe^{II}(catH)](X) (**1a**, L = 6-Me_3-TPA, catH = CatH; **1b**, L = 6-Me_3-TPA, catH = DBCH; **1c**, L = 6-Me_2-bpmcn, catH = CatH; **1d**, L = 6-Me_2-bpmcn, catH = DBCH) as pale greenish yellow solids in 60∼90% yield. These Fe(II)−catecholate complexes are very air-sensitive in solution and exhibit a strong and broad ν_{OH} band at around 3300 cm^{-1} in the solid state. The electronic spectra of these complexes show only one intense absorption band near 390 nm, which gives rise to their light yellow color. This feature likely arises from an iron(II)-to-pyridine charge-transfer transition, as the absorption intensities of **1a** and **1b** are twice as large as those of **1c** and **1d** due to the greater number of pendant pyridines. These Fe(II)−catecholate complexes react with O_2 to afford corresponding Fe(III)−catecholate complexes (**2**) which in turn undergo oxidative cleavage of the bound catecholate. In addition, reactions of the Fe(II) complexes with NO give rise to transient iron−nitrosyl intermediate adducts (**3**). Although these adducts

Scheme 1

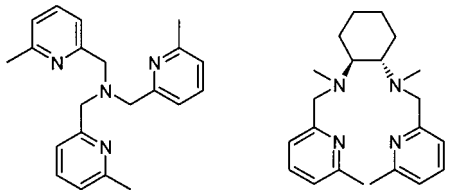

can be observed spectroscopically, they could not be isolated. Instead, **3a** and **3b** decompose to afford two distinct species: [(6-Me_3-TPA)Fe^{III}(cat)]$^+$ (**2a** and **2b**) and [(6-Me_3-TPA)Fe-$(NO)_2$]$^+$ (**4**) as final products, while **3d** yields only the corresponding Fe(III)−catecholate complex (**2d**). Scheme 2 summarizes the reactions of complexes **1** with O_2 and NO. The crystal structures of **1d**, **2a**, **2d**, and **4** were solved and are described below.

Scheme 2

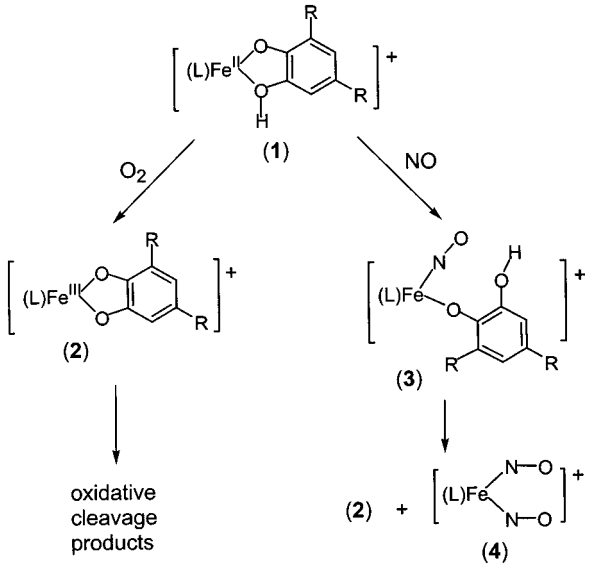

Table 2. Selected Bond Lengths (Å) for **1b**, **1d**, **2a**, and **2d**

	1b[a]	1d	2a	2d
Fe(1)−O(1)	2.263(8)	2.3443(13)	1.896(2)	1.926(2)
Fe(1)−O(2)	1.953(8)	1.9434(11)	1.972(2)	1.928(2)
Fe(1)−N(1)	2.21(1)	2.2505(14)	2.151(3)	2.193(3)
Fe(1)−N(2) [N(11)][#]	2.30(1)[#]	2.2405(14)	2.230(3)[#]	2.226(2)
Fe(1)−N(3) [N(21)][#]	2.172(9)[#]	2.2415(14)	2.248(2)[#]	2.217(2)
Fe(1)−N(4) [N(31)][#]	2.31(1)[#]	2.215(2)	2.202(3)[#]	2.269(3)
C(1)−O(1)	1.40(1)	1.396(2)	1.343(3)	1.345(3)
C(2)−O(2)	1.35(1)	1.339(2)	1.342(3)	1.348(3)
C(1)−C(2)	1.40(2)	1.401(2)	1.391(4)	1.402(4)

[a] Ref 7.

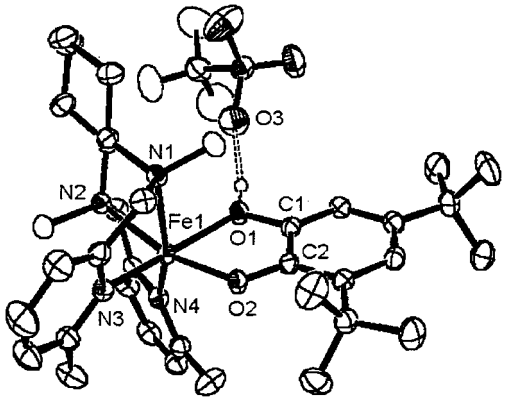

1d

Figure 1. ORTEP plot of [(6-Me_2-bpmcn)Fe(DBCH)](CF_3SO_3) (**1d**) showing 50% probability thermal ellipsoids and the labeling scheme for selected atoms. The dashed line shows the hydrogen bonding interaction (2.65 Å) between HO1 on the DBCH ligand and O3 on CF_3SO_3 anion. All other hydrogen atoms are omitted for clarity.

Structural Characterization. [(6-Me_2-bpmcn)Fe^{II}(DBCH)](CF_3SO_3) (1d). The crystal structure of **1d** is shown in Figure 1 with selected bond lengths listed in Table 2. This structure is comparable with that previously reported for [(6-Me_3-TPA)-Fe^{II}(DBCH)](ClO_4) (**1b**).[7] The iron center has a distorted octahedral environment with a tetradentate ligand and a bidentate catecholate ligand. The catecholate ligand binds to the iron asymmetrically with two distinct Fe−O bond lengths of 1.943(1) and 2.344(1) Å. The shorter Fe1−O2 bond is *trans* to the weaker amine ligand (N2), while the longer Fe1−O1 bond is *trans* to a pyridine nitrogen (N3). The 0.40 Å difference in Fe−O_{cat} bonds and the presence of one counterion per molecule unit strongly suggest that the catecholate ligand is a monoanion. Indeed the difference in Fe−O_{cat} bond lengths for **1d** is 0.09 Å larger than the 0.31 Å difference found for **1b**.[7] Deprotonation of the O2 oxygen is consistent with model studies,[10] showing that the O2 oxygen is the more basic ligand and affords a stronger interaction with the iron center. This deprotonation occurs despite potential steric interactions between the 3-*tert*-butyl group of the DBCH ligand and one of the α-methyl groups of the 6-Me_2-bpmcn ligand, so electronic factors appear more important than steric factors in determining which catechol oxygen becomes deprotonated. Furthermore the O1 oxygen is only 2.65 Å away from an oxygen atom of the counterion $CF_3SO_3^-$, suggesting a hydrogen bonding interaction which would stabilize the monoanionic form of the catecholate. The steric interactions among the α-methyl groups of 6-Me_2-bpmcn and the 3-*tert*-butyl group of DBCH ligand give rise to bond angles much larger than those that are associated with an ideal octahedron (O2−Fe1−N4 107.42(5)°, N3−Fe1−N4 111.89(5)°).

Scheme 3

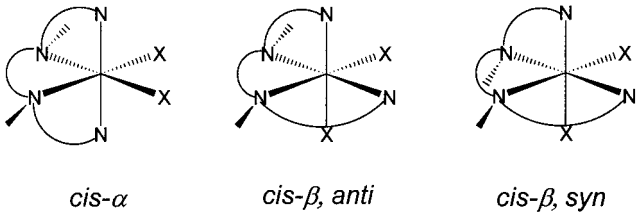

The Fe−N bonds of 6-Me_2-bpmcn have lengths of 2.22−2.25 Å, typical of α-methylpyridines coordinated to high-spin Fe(II) ions.[16] However, the coordination configuration of the 6-Me_2-bpmcn ligand differs from that of related ligands in mononuclear[17] and dinuclear iron complexes[18] such as [(L)-$Fe^{II}(CH_3CN)_2]^{2+}$, [(L)$Fe^{III}(\mu$-O)(μ-OH)Fe^{III}(L)]$^{3+}$, and [(L)-$Fe^{III}(\mu$-O)(μ-O_2CR)Fe^{III}(L)]$^{3+}$ (L = bpeen, bpmcn, bpmen; R = −H, $-CH_3$). In all these complexes, the tetradentate ligand coordinates to the metal center in a *cis*-α configuration, i.e., the two pyridyl groups are *trans* to each other as shown in Scheme 3. However, the 6-Me_2-bpmcn ligand in **1d** coordinates to the iron(II) center in a *cis*-β configuration, i.e., the two pyridyl groups are *cis* to each other. This distinct configuration may arise from the introduction of the α-methyl groups of 6-Me_2-bpmcn.

[(6-Me_3-TPA)Fe^{III}(Cat)](BPh_4) (2a) and [(6-Me_2-bpmcn)-Fe^{III}(DBC)](CF_3SO_3) (2d). The crystal structures of **2a** and **2d** are shown in Figure 2 and selected bond lengths are given in Table 2. The structure of **2a** is comparable to those of previously

(16) (a) Zang, Y.; Kim, J.; Dong, Y.; Wilkinson, E. C.; Appelman, E. H.; Que, L., Jr. *J. Am. Chem. Soc.* **1997**, *119*, 4197−4205. (b) Constable, E. C.; Baum, G.; Bill, E.; Dyson, R.; van Eldik, R.; Fenske, D.; Kaderli, S.; Morris, D.; Neubrand, A.; Neuburger, M.; Smith, D. R.; Wieghardt, K.; Zehnder, M.; Zuberbühler, A. D. *Chem. Eur. J.* **1999**, *5*, 498−508.

(17) (a) Chen, K.; Que, L., Jr. *Chem. Commun.* **1999**, 1375−1376. (b) Jo, D.-H. Unpublished observations.

(18) (a) Arulsamy, N.; Hodgson, D. J.; Glerup, J. *Inorg. Chim. Acta* **1993**, *209*, 61−69. (b) Glerup, J.; Goodson, P. A.; Hazell, A.; Hazell, R.; Hodgson, D. J.; McKenzie, C. J.; Michelsen, K.; Rychlewska, U.; Toftlund, H. *Inorg. Chem.* **1994**, *33*, 4105−4111. (c) Fenton, R. R.; Stephens, F. S.; Vagg, R. S.; Williams, P. A. *Inorg. Chim. Acta* **1995**, *236*, 109−115. (d) Glerup, J.; Michensen, K.; Arulsamy, N.; Hodgson, D. J. *Inorg. Chim. Acta* **1998**, *274*, 155−166. (e) Zheng, H.; Zang, Y.; Dong, Y.; Young, V. G., Jr.; Que, L., Jr. *J. Am. Chem. Soc.* **1999**, *121*, 2226−2235.

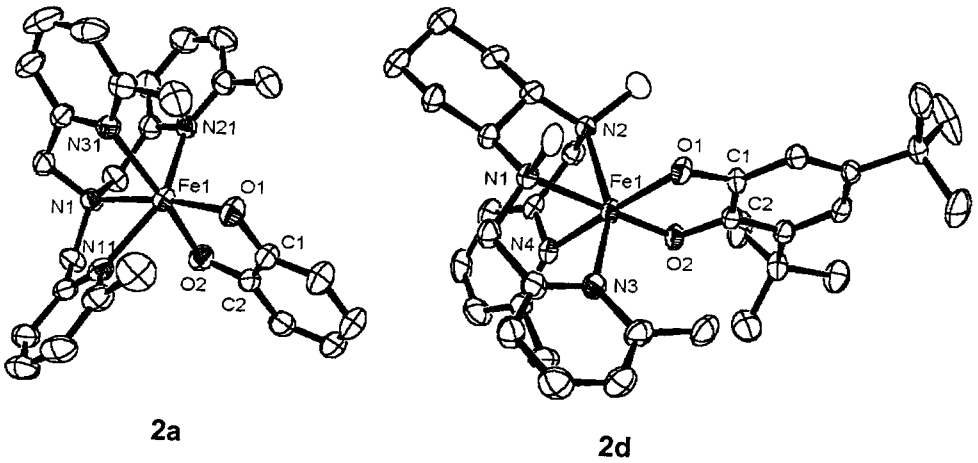

Figure 2. ORTEP plots of $[(6\text{-}Me_3\text{-}TPA)Fe(Cat)]^+$ (**2a**) and $[(6\text{-}Me_2\text{-}bpmcn)Fe(DBC)]^+$ (**2d**) showing 30% and 50% probability thermal ellipsoids, respectively, and the labeling scheme for selected atoms. Hydrogen atoms are omitted for clarity.

reported Fe(III)−catecholate complexes with tetradentate tripodal ligands.[10,11,19] The catecholate oxygens, N1 and N31, define an approximate plane of symmetry. As previously observed for Fe(6-Me_3-TPA) complexes,[16a,18e,20] the in-plane Fe1−N1 and Fe1−N31 bonds are shorter than the two out-of-plane Fe−N bonds, due to steric interactions among the α-methyl groups on the pyridine rings. For the same reason, the average $Fe-N_{py}$ bond length of **2a** (2.23 Å) is 0.1 Å longer than that of $[(TPA)Fe^{III}(DBC)](BPh_4)$ (2.13 Å). The catecholate ligand chelates to the iron asymmetrically with Fe−O bond lengths of 1.896(2) and 1.972(2) Å. This asymmetry ($\Delta r_{Fe-O} = 0.076$ Å) in **2a** is not as pronounced as in $[(NTA)Fe^{III}(DBC)]$ (0.092 Å)[19a] or $[(BPG)Fe^{III}(DBC)]$ (0.1 Å)[10] but is larger than in $[(TPA)Fe^{III}(DBC)]^+$ (0.019 Å).[11] Also, due to the steric congestion introduced by 6-Me_3-TPA, the bond angles related to O1 are larger than others (O1−Fe1−N11 100.27(10)°, O1−Fe1−N21 106.92(10)°, O1−Fe1−N31 107.46(10)°).

Complex **2d** also has a distorted octahedral geometry with average Fe−N and Fe−O bond lengths of 2.226(3) and 1.927(2) Å, respectively, typical of high-spin Fe(III) complexes.[16] Unlike in **2a**, the $Fe-O_{cat}$ bond lengths ($\Delta r_{Fe-O} = 0.002$ Å) are nearly identical. The larger bond angles, O2−Fe1−N3 110.01(9)° and N3−Fe1−N4 97.78(9)°, result from steric congestion among α-methyl groups of 6-Me_2-bpmcn and the 3-*tert*-butyl group of the DBCH ligand, as in **1d**. Surprisingly, although the 6-Me_2-bpmcn ligands in both **1d** and **2d** have the same *cis-β* topology, their conformations differ. While the two *N*-methyl groups in **1d** are *anti* to each other, those on **2d** are *syn*. The epimerization of the 6-Me_2-bpmcn ligand may result from steric interactions that develop upon oxidation of the metal center.

$[(6\text{-}Me_3\text{-}TPA)Fe(NO)_2](ClO_4)$ (4). The crystal structure of **4** is shown in Figure 3 and selected bond lengths and angles are listed in Table 3. Complex **4** has a trigonal bipyramidal iron center with two equatorial nitrosyl groups. The 6-Me_3-TPA ligand binds to the iron as a meridional tridentate ligand with one of the pyridine arms remaining unbound and just dangling away from the iron. As observed in other structures of Fe(6-Me_3-TPA) complexes,[16a,20−21] the axial $Fe-N_{py}$ bonds are somewhat elongated (2.251(3) and 2.207(3) Å) relative to the equatorial $Fe-N_{am}$ bond (2.160(3) Å) to minimize steric interactions between the α-methyl substituents on the pyridines.

The $Fe(NO)_2$ unit in the complex is nearly planar and the two NO ligands are almost equivalent crystallographically. The $Fe(NO)_2$ unit of **4** is characterized by shorter Fe−N and N−O bond lengths (average 1.695(3) and 1.167(4) Å, respectively)

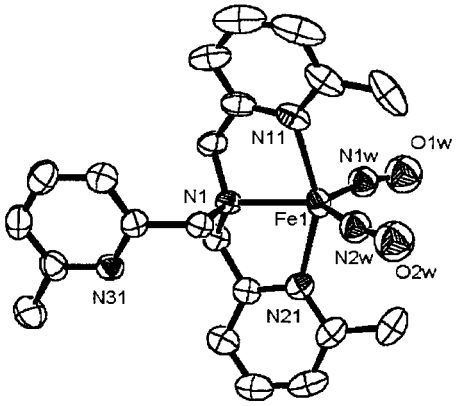

Figure 3. ORTEP plot of $[(6\text{-}Me_3\text{-}TPA)Fe(NO)_2]^+$ (**4**) showing 50% probability thermal ellipsoids and the labeling scheme for selected atoms. Hydrogen atoms are omitted for clarity.

Table 3. Selected Bond Lengths (Å) and Bond Angles (deg) for **4**

Fe(1)−N(1w)	1.699(3)	Fe(1)−N(2w)	1.690(3)
Fe(1)−N(1)	2.160(3)	Fe(1)−N(11)	2.251(3)
Fe(1)−N(21)	2.207(3)	N(1w)−O(1w)	1.168(4)
N(2w)−O(2w)	1.165(4)		
N(1w)−Fe(1)−N(2w)	110.4(2)	N(1w)−Fe(1)−N(1)	125.8(2)
N(1w)−Fe(1)−N(11)	99.7(2)	N(1w)−Fe(1)−N(21)	97.62(14)
N(2w)-Fe(1)−N(1)	123.8(2)	N(2w)−Fe(1)−N(11)	97.3(2)
N(2w)-Fe(1)−N(21)	96.4(2)	N(1)−Fe(1)−N(11)	75.60(12)
N(1)−Fe(1)−N(21)	76.97(11)	N(11)−Fe(1)−N(21)	152.52(12)
Fe(1)−N(2w)−O(2w)	162.4(4)	Fe(1)−N(1w)−(O1w)	159.7(4)

(19) (a) Que, L., Jr.; Kolanczyk, R. C.; White, L. S. *J. Am. Chem. Soc.* **1987**, *109*, 5373−5380. (b) Cox, D. D.; Benkovic, S. J.; Bloom, L. M.; Bradley, F. C.; Nelson, M. J.; Que, L., Jr.; Wallick, D. E. *J. Am. Chem. Soc.* **1988**, *110*, 2026−2032. (c) Koch, W. O.; Krüger, H.-J. *Angew. Chem., Int. Ed. Engl.* **1995**, *34*, 2671−2674. (d) Mialane, P.; Anxolabéhère-Mallart, E.; Blondin, G.; Nivorojkine, A.; Guilhem, J.; Tchertanova, L.; Cesario, M.; Ravi, N.; Bominaar, E.; Girerd, J.-J.; Münck, E. *Inorg. Chim. Acta* **1997**, *263*, 367−378. (e) Duda, M.; Pascaly, M.; Krebs, B. *Chem. Commun.* **1997**, 835−836. (f) Mialane, P.; Tchertanov, L.; Banse, F.; Sainton, J.; Girerd, J.-J. *Inorg. Chem.* **2000**, *39*, 2440−2444.

(20) (a) Chiou, Y.-M.; Que, L., Jr. *J. Am. Chem. Soc.* **1992**, *114*, 7567−7568. (b) Zang, Y.; Elgren, T. E.; Dong, Y.; Que, L., Jr. *J. Am. Chem. Soc.* **1993**, *115*, 811−813.

(21) (a) Zang, Y.; Jang, H. G.; Chiou, Y.-M.; Hendrich, M. P.; Que, L., Jr. *Inorg. Chim. Acta* **1993**, *213*, 41−48. (b) Chiou, Y.-M.; Que, L., Jr. *J. Am. Chem. Soc.* **1995**, *117*, 3999−4013.

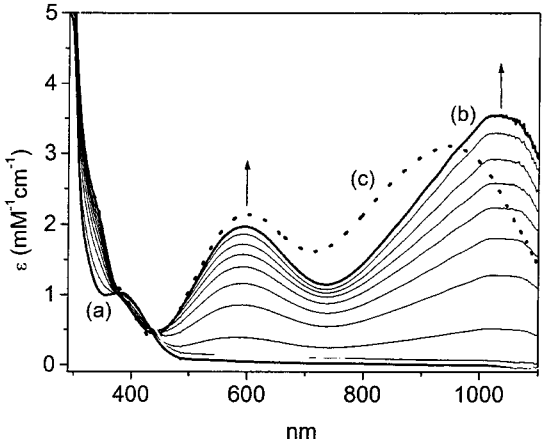

Figure 4. Absorption spectral changes for the reaction of **1d** with O_2 in CH_3CN at 22 °C. (a) Unreacted **1d**, (b) in situ formed **2d**, and (c) isolated **2d**.

than those of iron−mononitrosyl complexes.[22−24] The short Fe−NO distances indicate substantial covalent character between the iron and the nitrosyl ligands. The N1w−Fe1−N2w angle of 110.4(2)° is larger than the O1w−Fe1−O2w angle of 95.0(2)°, indicating that the iron−dinitrosyl group adopts an "*attracto*" conformation. The "*attracto*" conformation refers to the fact that the two NO ligands bend toward each other, usually observed for the first-low (3d) transition metal complexes containing good π-acceptor ligands.[22a] Complex **4** represents a species with an $\{Fe(NO)_2\}^9$ electronic configuration, thereby increasing the small number of structurally characterized $\{Fe(NO)_2\}^9$ complexes with nitrogen− and/or oxygen−donor ligands.[25]

Reactions of Fe(II)−Catecholate Complexes with O_2. The light yellow solutions of the Fe(II)−catecholate complexes (**1**) react immediately with O_2 to afford purple-blue intermediate species (**2**), the color of which arises from intense catecholate-to-Fe(III) LMCT bands (Figure 4, Table 4), as previously found for other [(L)Fe^{III}(catecholate)] (L = tetradentate ligands) complexes.[11,19] EPR spectra of **1a** and **1b** in CH_3CN show a strong and broad signal at $g = 12$ (Figure 5a), which is tentatively assigned to an integer-spin resonance arising from the $S = 2$ high-spin iron(II) center.[26] These features are replaced, upon exposure of **1a** and **1b** to O_2, by signals arising from high-spin iron(III) centers. Complexes **2a** and **2b** exhibit nearly axial EPR spectra, consisting of a major component with E/D = 0.06−0.065 and a minor component with E/D near 0 (Figure 5c, Table 4). Complex **2b** further reacts with O_2 to afford oxidative cleavage products (see below).

The spectral changes associated with the reaction of **1c** and **1d** with O_2 are more complex. The visible spectral changes for **1c** and **1d** are displayed in Figures S1 (Supporting Information) and 4, respectively. Interestingly, the LMCT bands of in situ

Table 4. Comparison of Properties of Fe(II)− and Fe(III)−Catecholate Complexes

complex	λ_{max} (ϵ)[a]	EPR (g)	E/D	k_{obs} (s^{-1})
1a	386 (2000)	12[b]		−
1b	395 (2200)	12[b]		1.1×10^{-2} [d]
1c	380 (900)	EPR-silent		1.7×10^{-2} [d]
1d	384 (1100)	EPR-silent		2.2×10^{-2} [d]
2a	540 (2100), 940 (3200)	7.3, 4.5, 1.9[b]	0.06	
		6.0	0	
2b	600 (2200), 1020 (3400)	7.5, 4.5, 1.9[b]	0.065	7.8×10^{-5} [e]
		6.0	0	
2c (in situ)	535 (2100), 950 (3100)	8.5, 5.6, 3.1[b]	0.13	
		6.3, 5.6, 2.0	0.02	
2c (isolated)	535 (2300), 874 (3000)	4.3[b]	0.33	
		8.4, 5.5, 3.0	0.13	
		6.3, 5.5, 2.0	0.02	
2d (in situ)	590 (2000), 1030 (3500)	8.4, 3.2[c]	0.13	2.7×10^{-5} [e]
		6.8, 5.2, 2.0	0.03	
2d (isolated)	598 (2200), 950 (3100)	9.3, 4.8, 4.1[c]	0.25	$<10^{-6}$ [e]
		8.4, 5.5, 3.0	0.13	

[a] Obtained in CH_3CN at 22 °C. [b] Obtained in CH_3CN at 5 K. [c] Obtained in CH_2Cl_2/toluene (2:1) at 5 K. [d] Rate constants for the formation of Fe(III)−catecholate complexes under 1 atm O_2 at 22 °C. [e] Rate constants for the decomposition of Fe(III)−catecholate complexes under 1 atm O_2 at 22 °C.

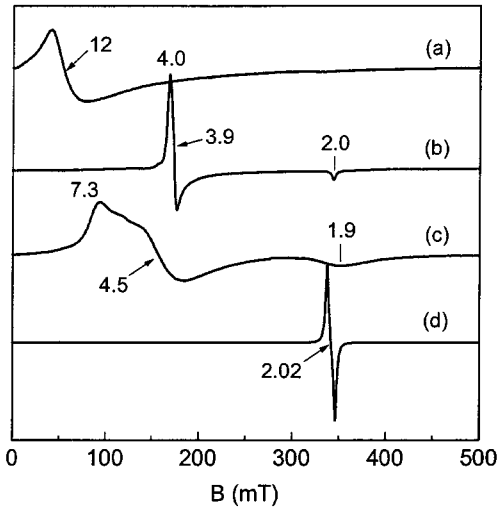

Figure 5. X-band EPR spectra in CH_3CN at 5 K of (a) **1a**, (b) iron−nitrosyl intermediate **3a** ($E/D = 0.006$), (c) **2a** ($E/D = 0.06$), and (d) **4**. Instrumental conditions: microwave power, 0.2 mW; microwave frequency, 9.63 GHz; modulation frequency, 100 kHz; modulation amplitude, 1 mT; gain, 60.

2c generated from the reaction of **1c** and O_2 are red-shifted from those of **2c** isolated from the same solution that was left standing in the refrigerator for several months (Figure S1b and c in Supporting Information). Similarly, the LMCT bands of **2d** generated in situ are also red-shifted relative to those of isolated **2d** (Figure 4 b and c), obtained upon long-term standing of in situ **2d** solutions generated either from the reaction of **1d** with a limited amount of O_2 or with NO (see below). Thus there appear to be two isomers of **2c** and **2d**, one that is generated directly in the reaction of **1c** or **1d** and O_2 and the other obtained upon long-term crystallization.

EPR studies support the notion of two forms of **2c** and **2d** (Table 4). Exposure of EPR-silent **1d** to O_2 immediately affords **2d** with EPR features associated with high-spin iron(III) $S = {}^5/_2$ species having E/D values of 0.03 and 0.13 (Figure 6c). In contrast, isolated **2d** has EPR features from an $E/D = 0.13$ species and a more rhombic $E/D = 0.25$ species (Figure 6d). Even crystals of **2d** exhibit signals from both $E/D = 0.13$ and

(22) (a) Enemark, J. H.; Feltham, R. D. *Coord. Chem. Rev.* **1974**, *13*, 339−406. (b) McCleverty, J. A. *Chem. Rev.* **1979**, *79*, 53−76. (c) Richter-Addo, G. B.; Legzdins, P. *Metal Nitrosyls*; Oxford University Press: New York, 1992.
(23) (a) Chiou, Y.-M.; Que, L., Jr. *Inorg. Chem.* **1995**, *34*, 3270−3278. (b) Ray, M.; Golombek, A. P.; Hendrich, M. P.; Yap, G. P. A.; Liable-Sands, L. M.; Rheingold, A. L.; Borovik, A. S. *Inorg. Chem.* **1999**, *38*, 3110−3115.
(24) Pohl, K.; Wieghardt, K.; Nuber, B.; Weiss, J. *J. Chem. Soc., Dalton Trans.* **1987**, 187−192.
(25) (a) Chong, K. S.; Rettig, S. J.; Storr, A.; Trotter, J. *Can. J. Chem.* **1979**, *57*, 3119−3125. (b) Chong, K. S.; Rettig, S. J.; Storr, A.; Trotter, J. *Can. J. Chem.* **1979**, *57*, 3113−3118. (c) Kisko, J. L.; Hascall, T.; Parkin, G. *J. Am. Chem. Soc.* **1998**, *120*, 10561−10562.
(26) Hendrich, M. P.; Debrunner, P. *Biophys. J.* **1989**, *56*, 489−506.

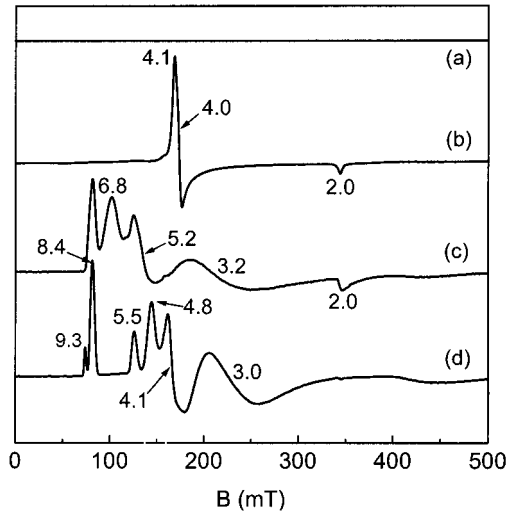

Figure 6. X-band EPR spectral changes observed in the reactions of **1d** with NO and O_2 at 5 K. (a) **1d** in CH_3CN, (b) iron−nitrosyl intermediate **3d** in CH_3CN ($E/D = 0.01$), (c) in situ formed **2d** ($E/D = 0.03, 0.13$) from the reaction of **1d** and O_2 in CH_2Cl_2/toluene (2:1), (d) isolated **2d** ($E/D = 0.13, 0.25$) in CH_2Cl_2/toluene (2:1) from the reaction of **1d** with NO. Instrumental conditions: microwave power, 0.2 mW; microwave frequency, 9.63 GHz; modulation frequency, 100 kHz; modulation amplitude, 1 mT; gain, 60.

0.26 species, as does **2d** obtained by direct synthesis. There is also a corresponding difference in the EPR properties of in situ generated **2c** and isolated **2c** (Figure S2 in Supporting Material). It is not unusual for high-spin iron(III) complexes to show E/D heterogeneity, which may arise from the sensitivity of the $S = {}^5/_2$ zero field splitting parameters to different conformations of the cyclohexane ring.[27] Despite the complexity of the EPR spectra, it is clear that in situ generated **2c** and **2d** are distinct from their isolated counterparts.

Most importantly, the reactivities of two forms of **2d** toward O_2 differ significantly. While the in situ generated complex reacts further with O_2 to afford about 90% yield of oxidative cleavage products (see below), isolated **2d** does not react with O_2 at all over a period of 4 days. Thus there must be a significant difference between the in situ generated and isolated forms of **2d**.

We propose the difference to arise from the two distinct ligand configurations found in the crystal structures of **1d** and **2d**, *cis-β, anti* for **1d** and *cis-β, syn* for **2d**. This structural difference reflects the epimerization of one *N*-CH_3 group in the conversion of **1d** to **2d**. However, this change entails breaking both an Fe−N_{am} and an Fe−N_{py} bond followed by rebinding with the inversion of the amine nitrogen and would be expected to have a large activation barrier. The in situ generated **2c** and **2d** are thus the kinetically controlled products, which retain the *cis-β, anti* configuration of the precursor complexes; they then must isomerize upon standing to form the thermodynamically more favored products having the *cis-β, syn* configuration observed in the crystal structure of **2d**.

Kinetic studies of the reaction of complexes **1** with O_2 were undertaken by monitoring the intensity changes of the LMCT bands of **2** under pseudo-first-order conditions in CH_3CN at 22 °C ($[O_2] = 8.1$ mM in CH_3CN under 1 atm pressure).[28] The

Scheme 4

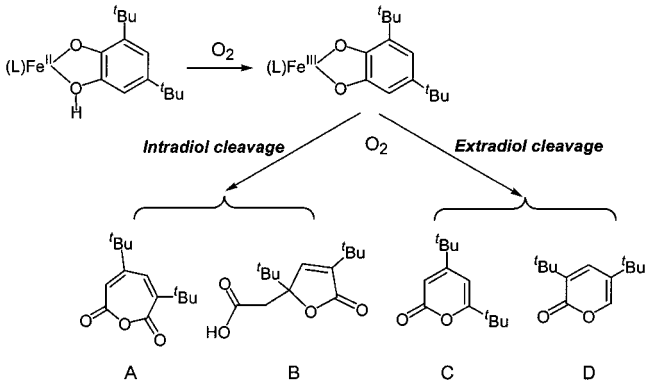

reactions consist of an initial fast formation of the blue chromophore, followed by a much slower first-order decay of the color (Figure 4 and Table 4). While the rates of formation are quite comparable for the three complexes studied, the rates of decomposition differ significantly. Not surprisingly, **2a** and **2c** are much more stable than **2b** and **2d** due to the absence of electron-donating *tert*-butyl groups. Complex **2b** and in situ generated **2d** react with O_2 with rates of $3-8 \times 10^{-5}$ s^{-1}, which are 3 orders of magnitude slower than that for $[(TPA)Fe^{III}(DBC)]^+$ (4.8×10^{-2} s^{-1} in DMF).[11] Although the metal centers in **2b** and **2d** have greater Lewis acidity, as indicated by their lower energy LMCT bands, we speculate that the steric hindrance introduced by 6-methyl substituents on the pyridines increases the barrier to the reaction. As noted earlier, isolated **2d** does not react with O_2 after 4 days, so the configuration of the tetradentate ligand also exerts a significant effect on the reactivity of the catecholate complex toward O_2. Given that the decay of in situ generated **2d** in the presence of O_2 is first order in **2d**, it would appear that the isomerization of in situ generated **2d** to isolated **2d** must be significantly slower than the reaction of in situ generated **2d** with O_2 to afford oxidative cleavage products.

As reported previously,[7] an O_2 uptake study for **1b** showed that 1.3(1) molecules of O_2 were consumed per molecule of **1b**. This result is consistent with 1 molecule of O_2 oxidizing 4 molecules of **1b** in the initial fast step (i.e. 0.25 O_2 per **1b** with O_2 being reduced to H_2O), and another molecule of O_2 cleaving the bound DBC on **2b** in the slower step. The reaction of **2b** with O_2 gives rise to mainly intradiol cleavage of the bound DBC in 89% yield. The major products observed are 3,5-di-*tert*-butyl-1-oxacyclohepta-3,5-diene-2,7-dione (A, 53%) and 3,5-di-*tert*-butyl-5-(carboxymethyl)-2-furanone (B, 36%), shown in Scheme 4. However, extradiol cleavage is also observed, accounting for 3% of the products. Both 4,6-di-*tert*-butyl-2-pyrone (C) and 3,5-di-*tert*-butyl-2-pyrone (D) are found. Similarly, the reaction of **2d** with O_2 results in 78(62:16)% intradiol cleavage and 12(4:8)% extradiol cleavage. Previous work has demonstrated that $[(L)Fe^{III}(DBC)]$ (L = tetradentate tripodal ligands) complexes afford exclusively intradiol cleavage products.[10,11,19] To date, extradiol cleavage has been observed only for complexes with facial tridentate ligands such as R_3-TACN and Tp^{i-Pr2}.[6,29] Thus, while it is expected that **2b** and **2d** yield predominantly intradiol cleavage products, it is surprising that there is a small amount of extradiol cleavage as well. Such cleavage may derive from complexes wherein one of the pyridyl arms has dissociated from the metal center. The steric congestion around the metal center engendered by the

(27) Simaan, J.; Poussereau, S.; Blondin, G.; Girerd, J.-J.; Defaye, D.; Philouze, C.; Guilhem, J.; Tchertanov, L. *Inorg. Chim. Acta* **2000**, *299*, 221−230.

(28) Sawyer, D. T. *Oxygen Chemistry*; Oxford University Press: New York, 1991; p 21.

(29) Jo, D.-H.; Que, L., Jr. *Angew. Chem., Int. Ed.* **2000**, *39*, 4284−4287.

Table 5. Comparison of Physicochemical Properties of Iron−Nitrosyl Adducts with $\{Fe(NO)_{1,2}\}^x$ ($x = 7, 9$) Configurations

complex[a]	Fe−NO (Å)	FeN−O (Å)	∠(Fe−N−O) (deg)	∠[Fe−(*N*O)$_2$] (deg)	∠[Fe−(N*O*)$_2$] (deg)	ν(NO) (cm^{-1})	reference
{Fe(NO)$_2$}^{9}							
4	1.690(3)	1.168(4)	159.7(4)	110.4(2)	95.0	1801, 1726	this work
	1.699(3)	1.165(4)	162.4(4)				
[(PhTp^{t-Bu})Fe(NO)$_2$]	1.688(3)	1.164(3)	166.8(3)	112.57(13)	99.8	1811, 1726	25c
	1.694(3)	1.172(3)	161.7(3)				
[(Pz$^{3,5-me2}$)Fe(NO)$_2$]$_2$ [b]	1.694(2)	1.159(2)	164.3(2)	110.6(1)	97.9	1802, 1780	25b
						1750, 1710	
[(GaPzO)Fe(NO)$_2$]	1.706(4)	1.158(5)	157.9(4)	108.1(2)	91.0	1724, 1671	25a
	1.700(4)	1.148(5)	159.3(5)				
{Fe(NO)}^{7}							
[(TPA)Fe(BF)(NO)]$^+$	1.72(2)	1.15(2)	159(2)	n.a.	n.a.	1794	23a
[(EDTA)Fe(NO)][c]	1.78	1.10	156(5)	n.a.	n.a.	1776	30
[(Me$_3$TACN)Fe(N$_3$)$_2$(NO)]	1.738(5)	1.142(7)	155.5(10)	n.a.	n.a.	1690	24

[a] PhTp^{t-Bu}, phenyl tris(3-*tert*-butylpyrazolyl)borate; Pz$^{3,5-me2}$, 3,5-dimethylpyrazolyl anion; GaPzO, dimethyl(*N*,*N*-dimethyl ethanolamino)(3,5-dimethyl-pyrazolyl)gallate[*N*(2),*N*(3),O]; BF, benzoylformate; EDTA, ethylenediaminetetraacetic acid; Me$_3$TACN, 1,4,7-trimethyl-1,4,7-triazacyclononane. [b] Average values. [c] Determined by using GNXAS analysis.

Scheme 5

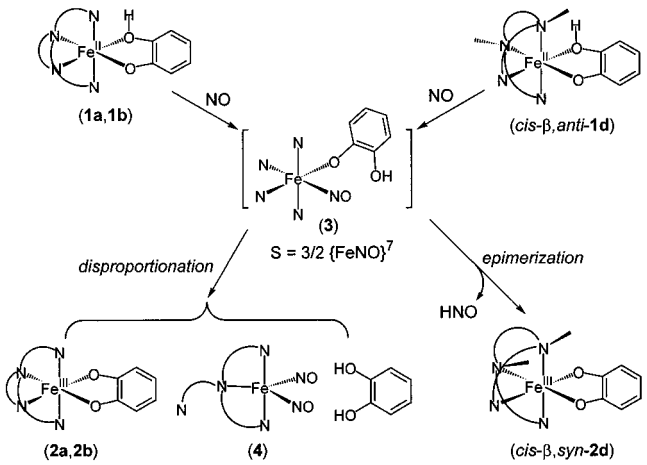

introduction of the 6-methyl substituent and resulting longer Fe−N$_{py}$ bonds may promote the dissociation. This would generate a site for O_2 attack at the metal center and result in extradiol cleavage, following a mechanism previously proposed for complexes of tridentate ligands.[6b,29]

Reactions of Fe(II)−Catecholate Complexes with NO. Scheme 5 summarizes the reactions of complexes **1** with NO. When NO is bubbled through a solution of **1** (CH_3OH for **1a** and CH_2Cl_2 for **1b**, **1d**) at 22 °C under anaerobic conditions, the initial light yellow color darkens to brown and then changes to purple-blue. These brown intermediate solutions (**3**) exhibit UV−vis absorption features near 400, 500, and 700 nm, typical of synthetic $S = {}^3/_2$ Fe−NO complexes (Table 6).[23,30] Intermediates **3** also show typical axial $S = {}^3/_2$ EPR signals, with $g =$ 4.0, 3.9, 2.0 for **3a** ($E/D = 0.006$) and 4.1, 4.0, 2.0 for **3d** ($E/D = 0.01$) (Figures 5b and 6b), accounting for >95% of the total spin in the samples. Thus the nitrosyl adducts of **1** can be formulated as [(L)Fe(catH)(NO)]$^+$ (**3**) with an $\{Fe(NO)\}^7$ electronic configuration. Unfortunately, none of the complexes **3** could be isolated due to their instability. Complexes **3a** and **3b** convert to two distinct products in comparable yields: deep-blue crystals of [(6-Me$_3$-TPA)Fe^{III}(cat)]$^+$ (**2a** and **2b**) and brown-red crystals of [(6-Me$_3$-TPA)Fe(NO)$_2$]$^+$ (**4**), while **3d** yields only the corresponding Fe(III)−catecholate complex (**2d**) in 90% yield (and presumably an equivalent of HNO). Similar to that observed for the reaction of **1d** with O_2, the reaction of **1d** with NO initially affords a **2d** product with *cis*-β, *anti* ligand configuration, as indicated by its UV−vis spectrum ($\lambda_{max} = 590$ and 1030 nm); this species then epimerizes upon long term standing to the thermodynamically more favored *cis*-β, *syn* configuration ($\lambda_{max} = 598$ and 950 nm).

Complex **4** exhibits a UV−vis spectrum with absorption shoulders at 332 (1700) and 374 (1300) nm and weak, broad bands at 460 (360) and 820 (200) nm. It has an IR spectrum with two intense nitrosyl stretching vibrations at 1801 and 1726 cm^{-1}, consistent with the presence of an Fe(NO)$_2$ moiety.[31] Its X-band EPR spectrum in a frozen CH_3CN solution (Figure 5d) shows only one intense isotropic signal at $g = 2.02$, which clearly indicates the presence of an $S = {}^1/_2$ species. The complex can thus be assigned as an $\{Fe(NO)_2\}^9$ system and is related to other iron−dinitrosyl complexes, which exhibit an isotropic $g = 2.03$ signal.[32] The formation of **4** is a result of the disproportionation of **3a** and **3b**, resulting in the transfer of NO and one electron from one iron center to another. The expected free catechol byproduct was found in the mother liquor.

Summary and Perspective

As part of our efforts to model extradiol cleaving catechol dioxygenases, we have prepared a series of Fe(II)−catecholate complexes (**1**) as structural mimics for the enzyme−substrate complexes. The bound catecholate is monoanionic but acts as a bidentate ligand. The fact that one oxygen is negatively charged while the other is neutral results in a coordination mode where the Fe−O$_{cat}$ bonds differ in length by as much as 0.4 Å. A similar coordination mode has thus been proposed for the catecholate substrate bound to catechol 2,3-dioxygenase, on the basis of the appearance of a short (1.93 Å) Fe−O bond upon substrate binding in the EXAFS analysis of this complex.[4] This notion is supported by more recent crystallographic data on the enzymes.[3] However the iron centers of the model complexes are six-coordinate, while those of the enzyme−substrate complexes are five-coordinate and thus have one available site for O_2 binding. Nevertheless the model complexes can react with

(30) Brown, C. A.; Pavlosky, M. A.; Westre, T. E.; Zhang, Y.; Hedman, B.; Hodgson, K. O.; Solomon, E. I. *J. Am. Chem. Soc.* **1995**, *117*, 715−732.

(31) (a) Beck, W.; Melnikoff, A.; Stahl, R. *Chem. Ber.* **1966**, *99*, 3721−3727. (b) Poletti, A.; Foffani, A.; Cataliotti, R. *Spectrochim. Acta* **1970**, *26A*, 1063−1069.

(32) (a) Bulter, A. R.; Glidewell, C.; Li, M.-H. *Adv. Inorg. Chem.* **1988**, *32*, 335−393. (b) Vanin, A. F. *FEBS Lett.* **1991**, *289*, 1−3. (c) Kennedy, M. C.; Gan, T.; Antholine, W. E.; Petering, D. H. *Biochem. Biophys. Res. Commun.* **1993**, *196*, 632−635. (d) Butler, A. R.; Flitney, F. W.; Williams, D. L. H. *Trends Pharmacol. Sci.* **1995**, *16*, 18−22. (e) Noguchi, T.; Honda, J.; Nagamune, T.; Sasabe, H.; Inoue, Y.; Endo, I. *FEBS Lett.* **1995**, *358*, 9−12. (f) Muller, B.; Kleschyov, A. L.; Stoclet, J. C. *Br. J. Pharm.* **1996**, *119*, 1281−1285.

Table 6. UV−vis Spectral Features of Iron−Nitrosyl Adducts with $\{Fe(NO)\}^7$ Configuration[a]

complex	λ_{max} (ϵ)	reference
3a	360 (2600), 500 (720), 718 (440) 372 (2300) 388 (1700)	this work
3d	360 (2400), 550 (250), 750 (150) 372 (2500) 390 (2450)	this work
$[(6\text{-}Me_3\text{-}TPA)Fe(BF)(NO)]^+$	358 (1900), 492 (720), 690 (240) 372 (1600) 388 (1200)	23a
$[(TPA)Fe(BF)(NO)]^+$	350 (1100), 520 (250), 654 (160) 420 (730)	23a
[(EDTA)Fe(NO)]	340 (1300), 430 (900), 640 (200)	30

[a] Obtained in CH_3CN at 22 °C.

O_2 and NO. With NO, $S = {}^3/_2$ $\{Fe(NO)\}^7$ adducts are formed, as for the enzymes,[5] although the biomimetic adducts are susceptible to decomposition. The weaker $Fe-OH_{cat}$ bond is presumably easily broken and NO replaces it. On the other hand, exposure of complexes **1** to O_2 results in their immediate one-electron oxidation to the corresponding iron(III)−catecholate dianion complex, a reactivity pattern distinct from that of the enzymes.

These iron(III)−catecholate complexes further react with O_2 to afford oxidative cleavage products. Like previously reported iron(III)−catecholate complexes of tetradentate ligands, the major products derive from intradiol cleavage.[10,11,19] However, unlike the latter complexes, some extradiol cleavage is observed. Biomimetic extradiol cleavage has thus far been observed only for five-coordinate iron(III)−catecholate complexes.[6,29] So we speculate that, due to steric congestion around the iron center, there is a subpopulation of complexes with one pyridyl arm dissociated that gives rise to the minor products. Our model complexes to date are thus imperfect. Future efforts will be directed at obtaining five-coordinate iron(II)−catecholate complexes that react with O_2 and afford extradiol cleavage directly.

Acknowledgment. This work was supported by the National Institutes of Health (Grant GM-33162). D.-H.J. is grateful to the Korean Science and Engineering Foundation (KOSEF) for a postdoctoral fellowship. We thank Prof. Doyle Britton, Dr. Victor G. Young, Jr., and Dr. Maren Pink of the University of Minnesota X-ray Crystallographic Laboratory for determining the crystal structures of **1d**, **2a**, **2d**, and **4**.

Supporting Information Available: Crystallographic data for **1d**, **2a**, **2d**, and **4** (CIF format) and Figures S1 and S2 showing UV−vis and EPR spectral changes for **2c** (PDF format). These materials are available free of charge via the Internet at http://pubs.acs.org.

IC001185D